BIOLOGICAL
CRYSTALLOGRAPHY

Volume 71 (2015)

Supporting information for article:

Structure and catalytic mechanism of the evolutionarily unique bacterial chalcone isomerase

Maren Thomsen, Anne Tuukkanen, Jonathan Dickerhoff, Gottfried J. Palm, Hanna Kratzat, Dmitri I. Svergun, Klaus Weisz, Uwe T. Bornscheuer and Winfried Hinrichs

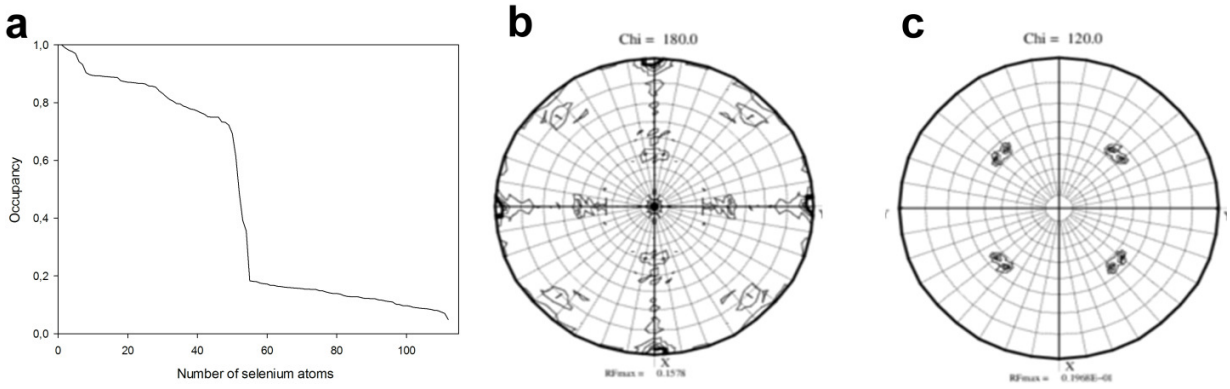

Figures S1 | Phasing and packing information. a, Occupancy of the Se positions of selenomethionine labelled CHI found with *SHELXD* (Sheldrick, 2010). Self-rotation function of native CHI diffraction data calculated with *MOLREP* (Vagin & Teplyakov, 2010; Winn *et al.*, 2011) in space group $I2_12_12_1$ at, **b**, chi = 180°, and, **c**, chi= 120° revealing three independent twofold and two threefold non-crystallographic axes.

Table S1 | Sequences of primers used to introduce desired mutations.

Primer name	Sequence
pET28b_CHI_H33A	5'-TAAAGTAGCGATTCCGGACAGC-3'
pET28b_CHI_H33E	5'-TAAAGTAGAAATTCCGGACAGC-3'
pET28b_CHI_H33Q	5'-TAAAGTACAGATTCCGGACAGC-3'
pET28b_CHI_H73A	5'-GCAGCTGACAGAGGCGCACTGGTTAG-3'
pET28b_CHI_Y48F	5'-CCAAATTTGCATTTTATCCGTCC-3'
pET_RP	5'-CTAGTTATTGCTCAGCGG-3'
pET28b_CHI_Δlid_fw	5'-GATCCCGGCAGCAGCAGAAGGAAATCC -3'
pET28b_CHI_Δlid_rv	5'-GGATTTCCTTCTGCTGCTGCCGGGATC -3'
pET28b_CHI_ΔC-terminus_fw	5'-GCGGCCGCTTATCTCATGGTGATTTATCC-3´
pET28b_CHI_ΔC-terminus_rv	5'-GGATAAATCACCATGAGATAAGCGGCCGC-3´

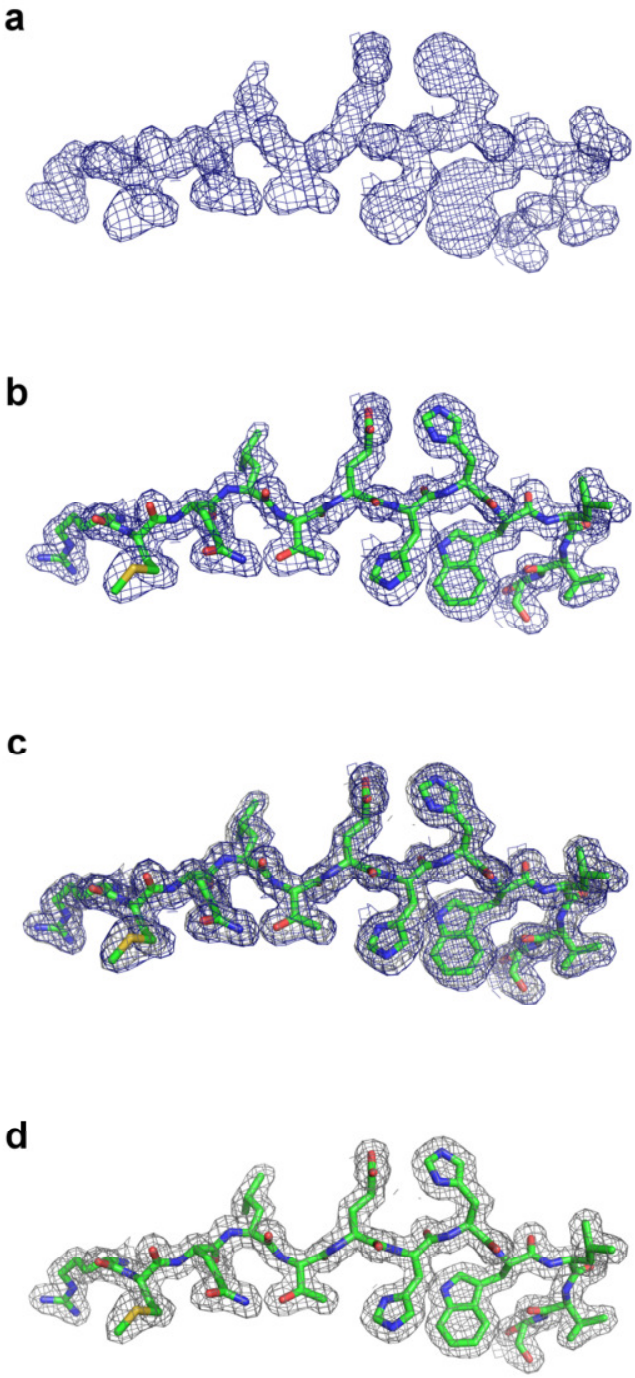

Figures S2 | Electron density maps shown for residues R67 – S78 of chain B. All maps are contoured at 1σ. **a**, Experimental F_{obs}-map obtained with *SHELXC/D/E* via SIRAS protocol coloured in blue. **b**, Experimental F_{obs}-map superposed with final model (PDB entry 4c9s) shown as stick model. **c**, Superposition of experimental F_{obs}-map (blue) and $2F_{obs} - F_{calc}$ electron density map (grey) after refinement and final model. **d**, Final model and final $2F_{obs} - F_{calc}$ electron density map.

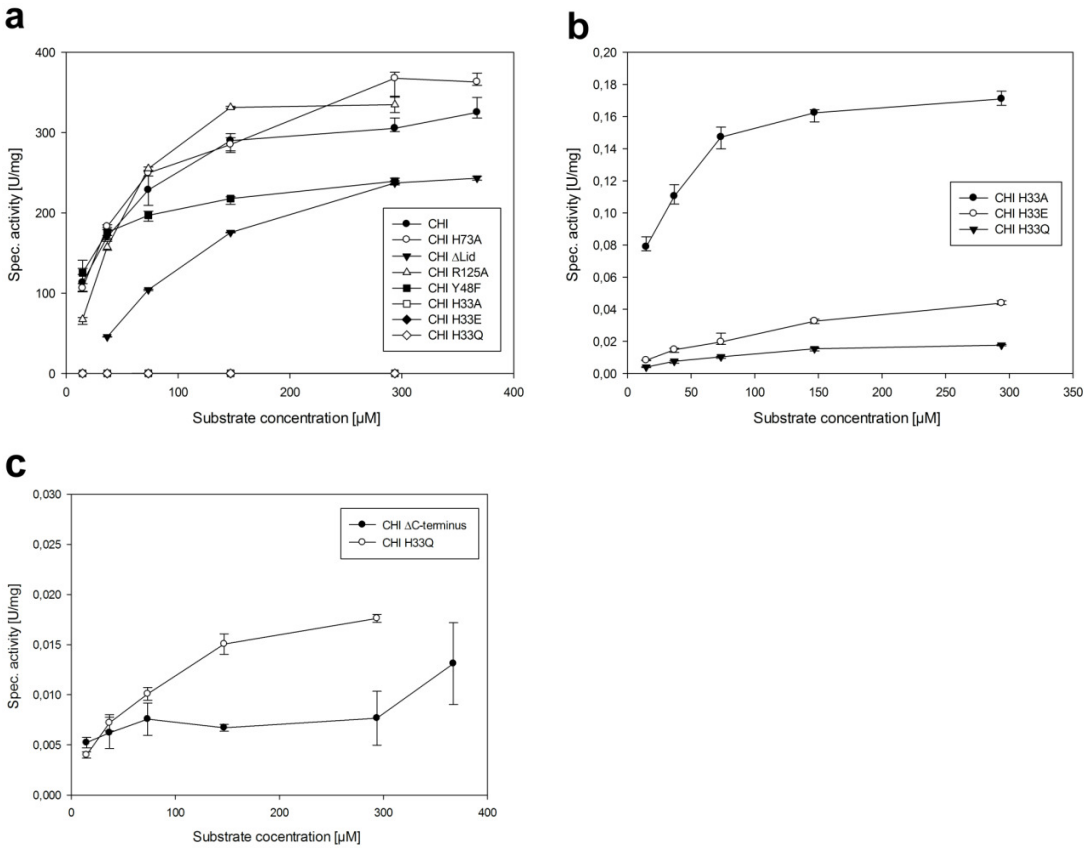

Figures S3 │ Enzymatic activity of CHI variants. a, The contribution of supposed catalytic residues of CHI for the conversion of naringenin chalcone to (2*S*)-naringenin is determined. **b**, The CHI variants H33A, H33E, and H33Q showed significantly reduced activity. **c**, The C-terminal truncated variant CHI_ΔC-terminus (missing residues 278 – 282) is less active than CHI_H33Q and still behaves as hexamer in gel-filtration, but is much less stable than the wild-type CHI.

Table S2 │ Melting points (T_m) of CHI.

Protein	**T_m [°C]**
CHI	47.9 ± 0.3
CHI_ΔC-term	39.0 ± 1.2

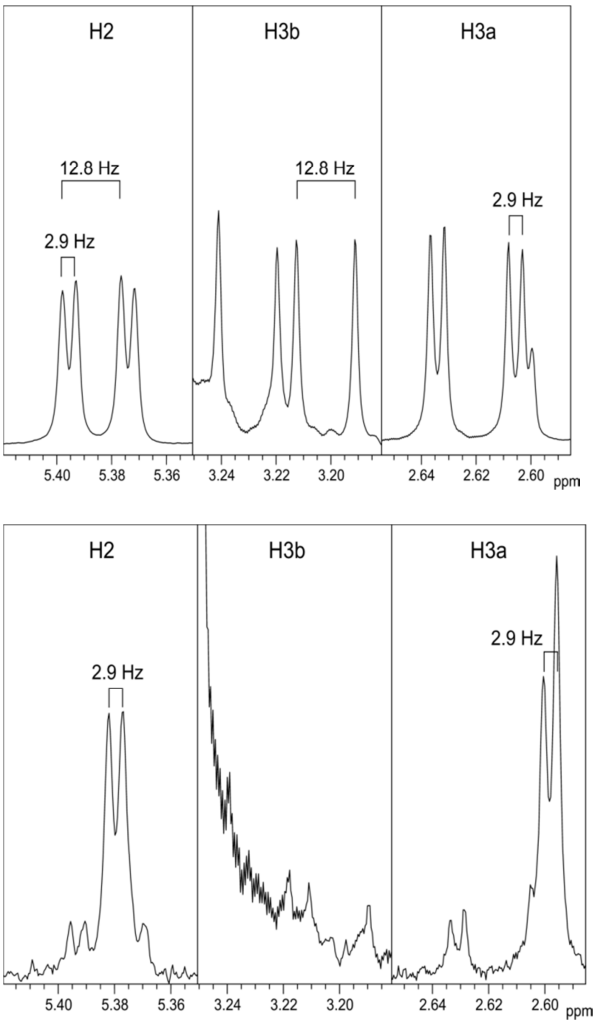

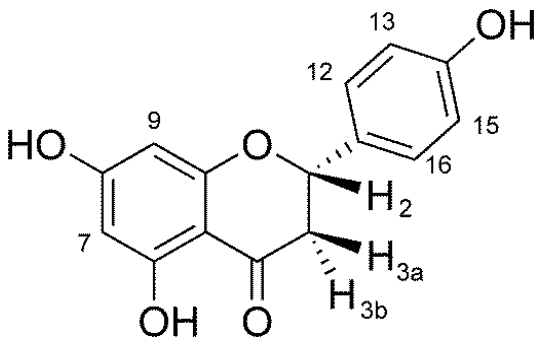

Figures S4 | Mechanistic studies with ^{1}H-NMR measurements. ^{1}H NMR spectral regions of (2*S*)-naringenin (top) enzymatically produced in H_2O (middle) and in D_2O (bottom). The signal of the proton H3b at the *pro*-S position of C3 is mostly lost through H/D exchange in D_2O solution, confirming its participation in the catalytic cycle.

(2*S*)-Naringenin: ^{1}H NMR (600 MHz, DMSO-d_6): δ (ppm) = 2.62 (1H, d/d, J = 2.9 Hz, 17.1 Hz, H3a), 3.22 (1H, d/d, J = 12.8 Hz, 17.1 Hz, H3b), 5.38 (1H, d/d, J = 2.9 Hz, 12.8 Hz, H2), 5.82 (2H, s, H7, H9), 6.73 (2H, d, J = 8.5 Hz, H13, H15), 7.26 (2H, d, J = 8.5 Hz, H12, H16), 9.55 (1H, s, OH), 10.75 (1H, s, OH), 12.10 (1H, s, OH).

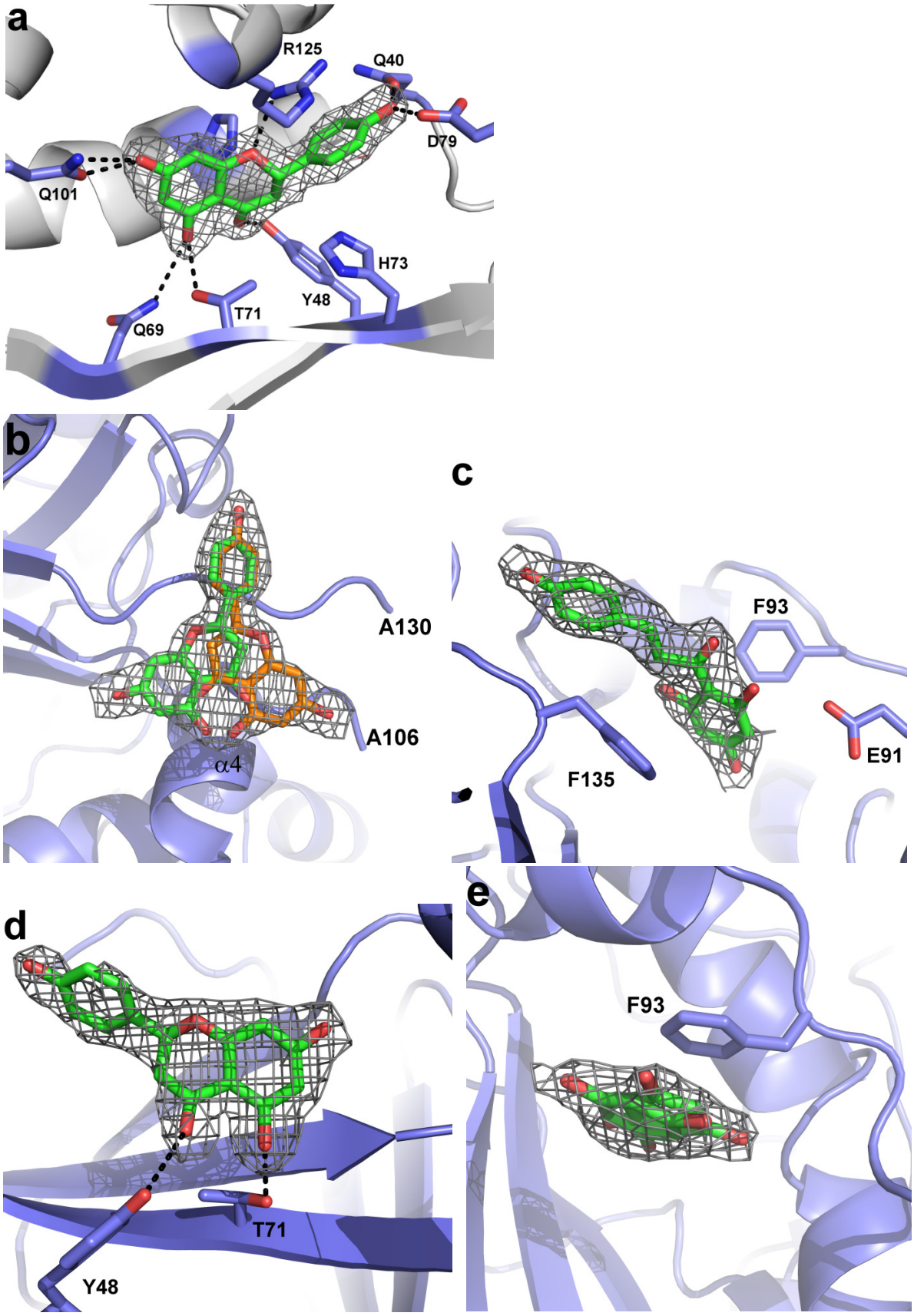
a
R125
Q40
D79
Q101
H73
Y48
T71
Q69
b
A130
A106
α4
c
F93
E91
F135
d
T71
Y48
e
F93

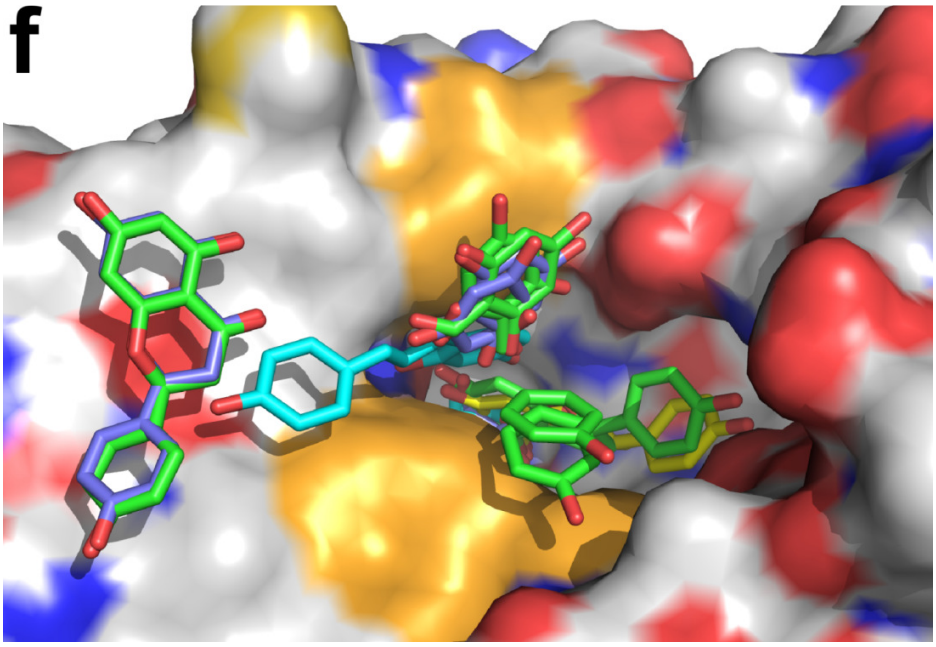

Figures S5a-f | Various substrate and product binding motifs. In all CHI monomers with open or closed lid several binding motifs of substrate (naringenin chalcone) and product ((2*S*)-naringenin) are observed in the active site and in the entry tunnel. This is due to the artificial high naringenin chalcone concentration for co-crystallization. The trimer with open conformation (monomers B, D, F) shows several additional binding motifs. The $2F_{obs} - F_{calc}$ electron density maps are contoured at 1σ level.

a, (2*S*)-naringenin in the active site as observed for monomers with closed lid (A, C, and E).

b, (2*S*)-naringenin on a crystallographic two-fold axis between the monomer D and its symmetry mate (−x, −y + ½, z). This is also detected (not shown) between monomer F and its symmetry mate (−x + ½, y, −z).

c, Naringenin chalcone bound in the entry region of the active site of monomer B (open lid).

d, (2*S*)-naringenin in the active site of monomer D that has an open lid conformation.

e, Alternative positions of the di-phenolic fragment in monomer F.

f, Superimposition of all CHI monomers with observed substrate or product sites. The surface of monomers with open lid conformations (here D) is show as template. Ligands of monomer B (cyan), of monomer D (green), and of monomer F (blue) are shown as stick models. The active site bound naringenin (yellow sticks) observed in monomers A, C, and E (all in closed conformations) is shown for comparison. The surfaces of the interacting hydrophobic residues F93, F135 and F137 are highlighted in orange.

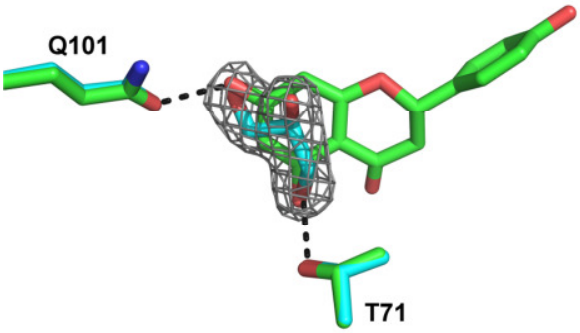

Figure S6 | Glycerol replacing the hydrogen bonds of the phenolic 4',6'-dihydroxy-fragment of the flavanone. Superposition of monomer A of the (2*S*)-naringenin complex and substrate-free CHI (side chains with yellow and light blue C-atoms, respectively). The local $2F_{obs} - F_{calc}$ electron density map of glycerol contoured at 1σ is shown.

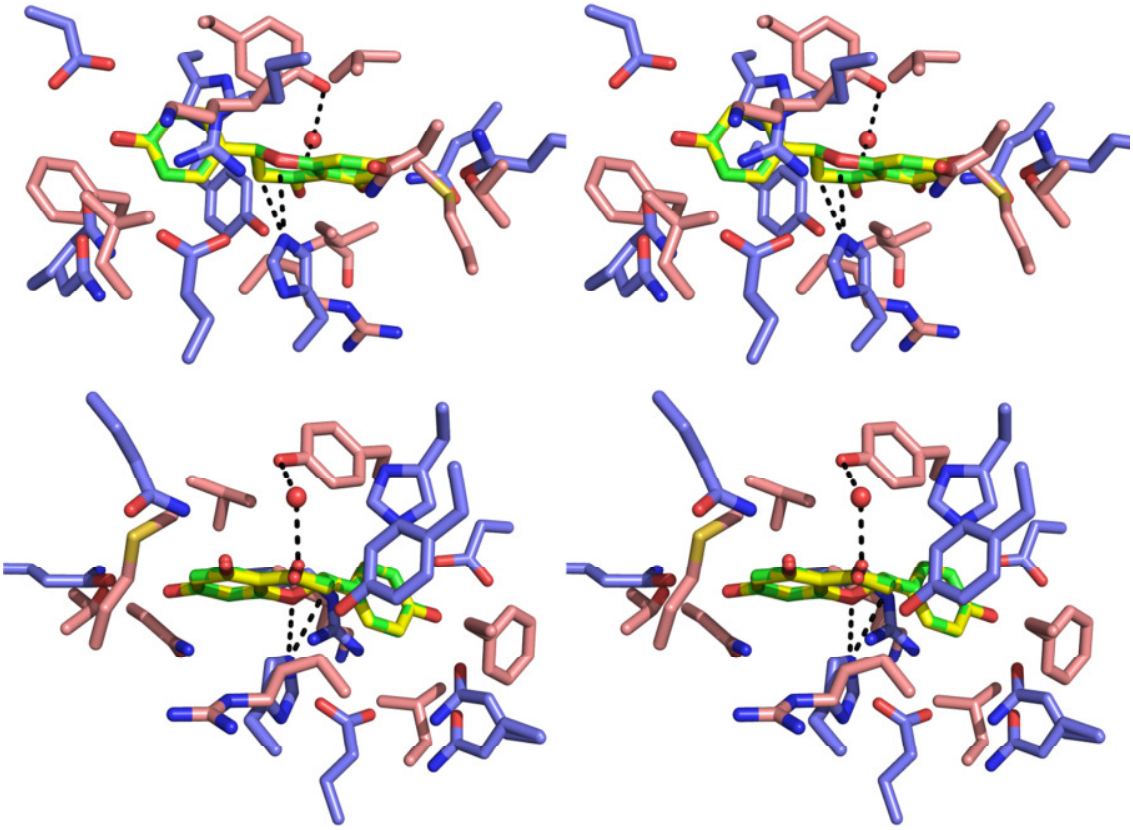

Figures S7 | Stereo views for comparison of the active site architecture of the chalcone isomerases of plant and the bacterial enzyme. Superposition performed based on substrate (2*S*)-naringenin (bacterial: green; plant: yellow) shows that there is no homology in substrate binding. The substrate binding in the plant enzyme (light rose) is based mainly on hydrophobic interactions whereas in the bacterial enzyme (blue) the substrate is coordinated via hydrogen bonds to the hydroxyl groups of naringenin. Notably, the catalytic responsible water molecule of the plant enzyme lies on the other site of the substrate compared to the catalytic responsible H33 of the bacterial enzyme. Stippled lines are the direct contact by hydrogen bonds to the substrate assumed for initiation of the oxa-Michael addition.

Table S3 | Overview of the secondary structure alignments performed with PDBeFold (Krissinel & Henrick, 2004). Sequence alignment with SCOPE (Fox *et al.*, 2014) identified no related proteins.

CHI domain	superposed on (PDB entry)	RMSD on Cα-atoms (Å)	Aligned with residues (of target protein)	Q-score
CHI, solvent exposed domain	SP1 (1TR0)	2.37	89 (106)	0.30
CHI, catalytic domain	SP1 (1TR0)	2.94	75 (106)	0.25
CHI, catalytic domain	CHI, solvent exposed domain	2.54	79 (152)	0.22
CHI, catalytic domain	chlorite dismutase (3Q08)	3.22	70 (241)	0.20
CHI, monomer	monooxygenase ACTVA-ORF6 (1N5V)	2.71	85 (258)	0.14
CHI, monomer	chlorite dismutase (3Q08)	4.68	170 (241)	0.13
CHI, monomer	plant CHI from *Medicago sativa* (1EYP)	2.72	74 (212)	0.055
CHI, monomer	fatty acid binding protein from *Arabidopsis thaliana* (4DOI)	2.86	73 (221)	0.049

SAXS experiments

Table S4 | SAXS Data Collection and Model-free Parameters.

Data collection parameters	CHI	naringenin-CHI	CHI_Δlid
Instrument	P12 at EMBL/DESY, storage ring PETRA III, Germany		
Beam geometry	0.2 × 0.12 mm^2		
Wavelength (Å)	1.24		
q-range (Å^{-1})	0.008 – 0.47		
Exposure time (ms)	20 × 50		
Concentration range (mg ml^{-1})	0.1 – 18.2	0.8 – 2.6	1.3 – 9.8
Temperature (K)	283	283	283
*Structural parameters**			
$I(0)$ (arbitrary units) (from $P(r)$)	25450 ± 10	24640 ± 10	26710 ± 10
R_g (from $P(r)$) (Å)	37 ± 2	36 ± 2	35 ± 2
$I(0)$ (arbitrary units) (from Guinier)	25450 ± 30	25100 ± 20	27220 ± 20
R_g (Å) (from Guinier)	36 ± 3	37 ± 3	36 ± 3
D_{max} (Å)	130 ± 5	110 ± 5	110 ± 5
Porod volume (10^3 Å^3)	320 ± 20	320 ± 20	270 ± 20
*Molecular mass determination**			
MM$_{POROD}$ (from Porod volume) (kDa)	190 ± 10	190 ± 10	160 ± 10
Contrast ($\Delta\rho$ × 10^{10} cm^{-2})	3.047	3.047	3.047
MM$_{saxs}$ (from $I(0)$, (kDa)	190 ± 20	190 ± 20	150 ± 10
Calculated hexameric MM from sequence (kDa)	194.4	194.4	181.2
SASBDB entry code	SASDAL6	SASDAM6	SASDAN6
Software employed			
Primary data reduction	Automated radial averaging (Petoukhov *et al.*, 2007)		
Data processing	PRIMUS (Konarev *et al.*, 2003)		
Ab initio analysis	DAMMIN (Svergun, 1999)		
Validation and averaging	DAMAVER (Volkov & Svergun, 2003)		
Rigid body modelling	CORAL (Petoukhov *et al.*, 2012)		
Computation of model intensities	CRYSOL (Svergun *et al.*, 1995)		

*Reported for infinite dilution of concentration series measurements

SAXS results

Small-angle X-ray scattering experiments (SAXS) of the wild-type CHI, its naringenin complex and the CHI_Δlid variant clearly show differences caused by lid deletion or lid closing upon naringenin binding.

1. Native CHI without naringenin ligand, theoretical MW = 194 kDa

SAXS of the native protein without ligands indicate no ionic strength dependent oligomerization (range of 0 – 1.0 M NaCl). The SAXS-based molecular mass estimates confirm hexameric assembly observed in the crystallographic structures. A*b initio* models of CHI are in excellent agreement with the overall shape of the high-resolution structure. The normalized spatial discrepancy (NSD) values for P1 and P6 reconstructions are 0.94 and 1.03, respectively (Kozin & Svergun, 2001). However, the theoretical scattering based on the crystallographic hexamer structure and addition of the missing lids using a single conformation does not fit the experimental SAXS data ($\chi = 3.4$).

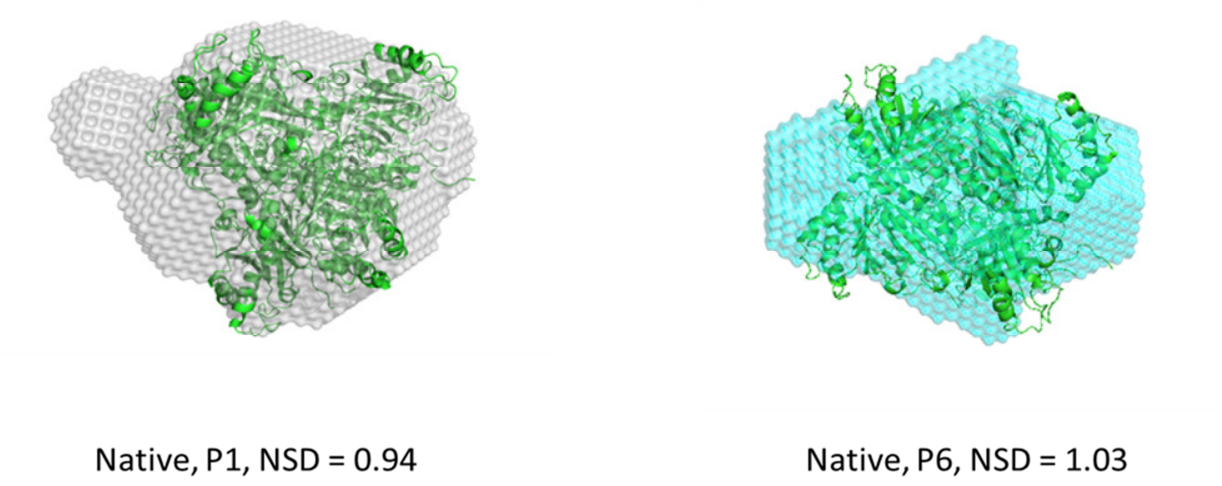

Figure S8 | The *ab initio* models in P1 and P6 symmetries. *Ab initio* models based on SAXS data have an excellent agreement with the crystallographic structure. The normalized spatial discrepancy (NSD) values for P1 and P6 reconstructions are given.

2. CHI with naringenin ligand, theoretical MW = 194 kDa

The overall structure of the ligand complex of CHI is more compact than that of the native protein that was observed as differences in R_g and D_{max} values. In addition, there is a change of the minimum of the SAXS profile of around ~ 0.1 $Å^{-1}$ indicating further a more globular structure than the ligand-free protein has. The structure with all loops closed (constructed using the crystallographic trimer model with closed loops in the crystallographic structure and symmetry operations) yielded a goodness-of-the-fit values of $\chi = 1.0$ with the experimental data.

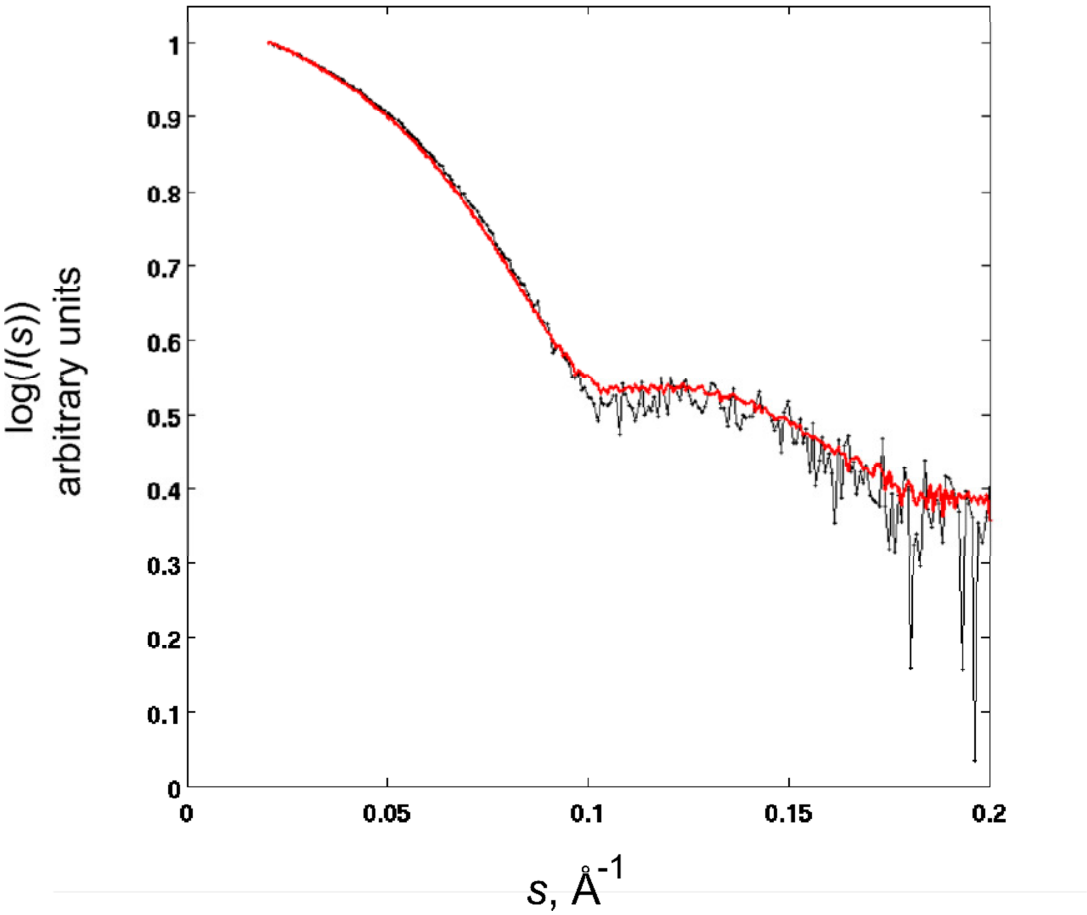

Figure S9 | SAXS data ccomparison of CHI in the absence (red) and presence (black) of naringenin. Concentrations used are as following 13.5 µM CHI, 1 mM naringenin.

3. CHI_Δlid variant, theoretical MW = 181 kDa

The observed R_g of the deletion mutant CHI_Δlid (missing amino-acid residues His109 – Ala130) is in accordance with the expectations. The best CRYSOL fit was obtained with the hexameric structure which is missing the lids regions ($\chi = 1.4$).

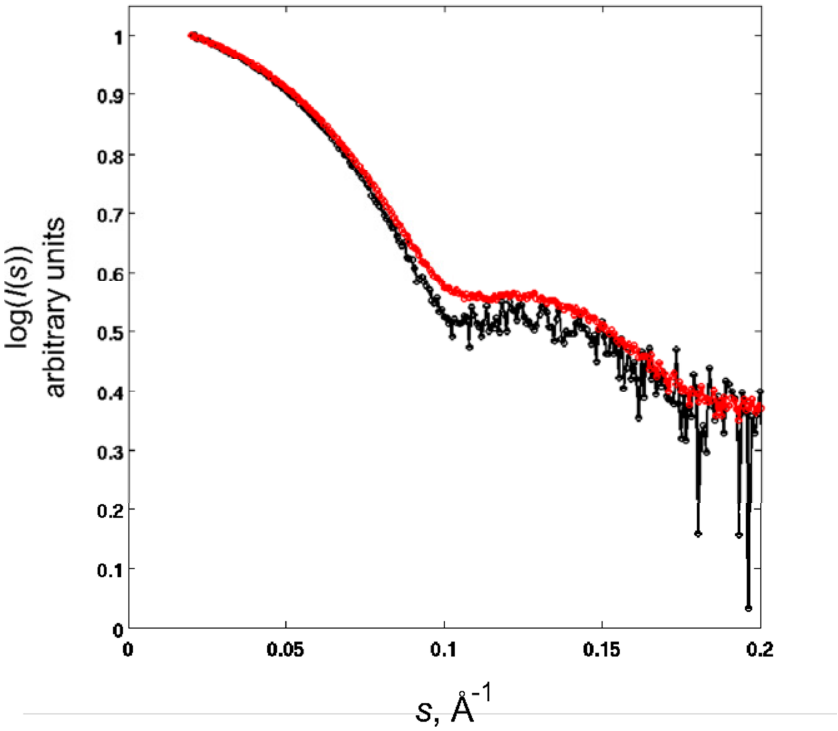

Figure S10 │ SAXS data comparison of the naringenin complex of CHI (red line) with CHI_Δlid (black line). Concentrations used are as following 13.5 µM CHI, 1 mM naringenin.

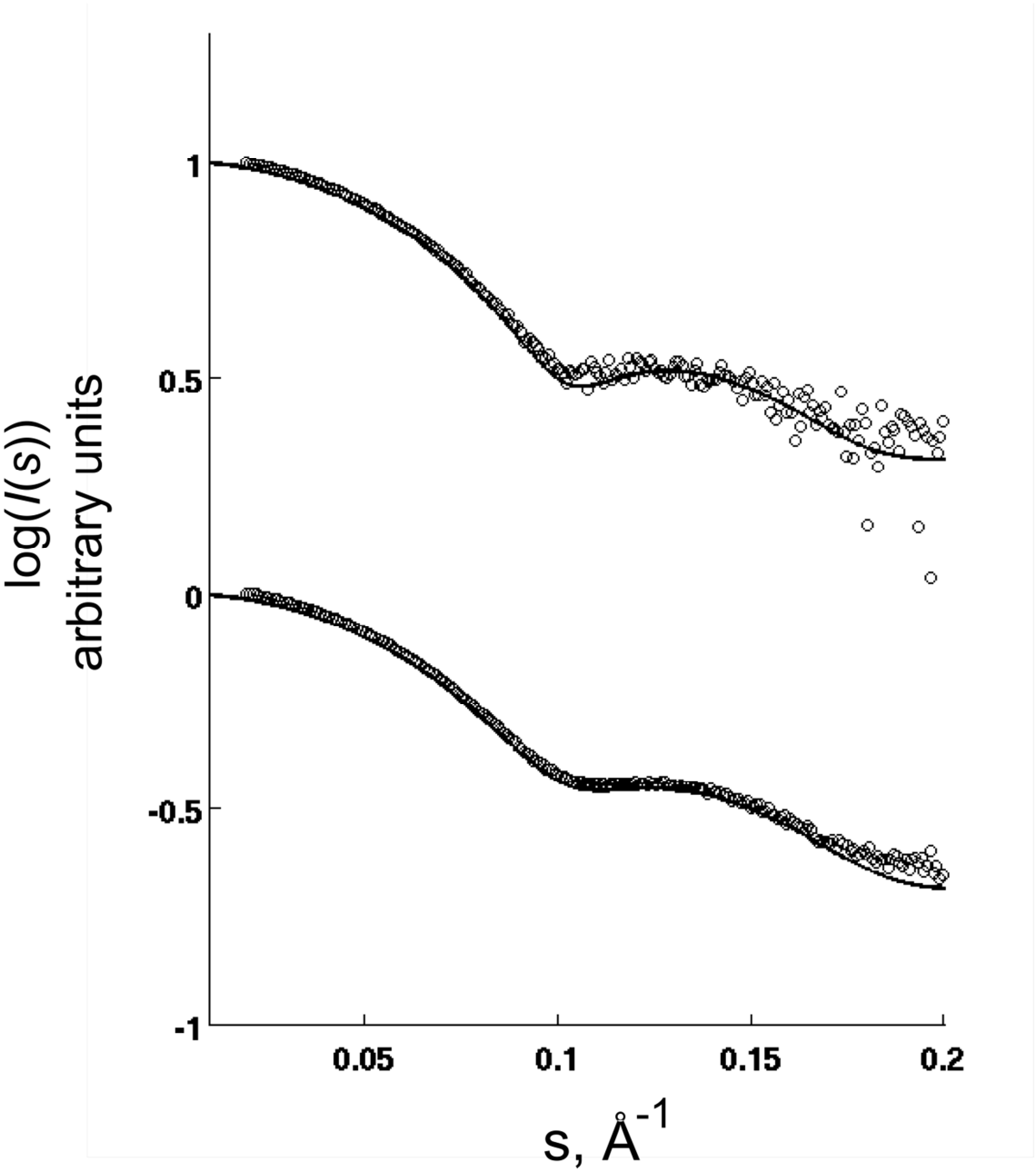

Figure S11 | CRYSOL fits of the naringenin-bound and unbound CHI structures (PDB codes 4d06 and 4c9s, resp.) to the SAXS data measured in the presence of 1mM naringenin (upper curve) and on the CHI_Δlid variant (lower curve). The goodness-of-the-fit values χ are 1.0 and 1.4 for the ligand-bound and unbound structures, respectively.

References

Fox, N. K., Brenner, S. E., Chandonia, J.-M. (2014). *Nucleic Acids Res.* **42**, D304-D309.

Konarev, P. V., Volkov, V. V., Sokolova, A. V., Koch, M. H. J., Svergun, D. I. (2003). *J. Appl. Crystallogr.* **36**, 1277-1282.

Kozin, M. B., Svergun, D. I. (2001). *J. Appl. Crystallogr.* **34**, 33-41.

Krissinel, E., Henrick, K. (2004). *Acta Cryst.* D**60**, 2256-2268.

Petoukhov, M. V., Franke, D., Shkumatov, A. V., Tria, G., Kikhney, A. G., Gajda, M., Gorba, C., Mertens, H. D. T., Konarev, P. V., Svergun, D. I. (2012). *J. Appl. Crystallogr.* **45**, 342-350.

Petoukhov, M. V., Konarev, P. V., Kikhney, A. G., Svergun, D. I. (2007). *J. Appl. Crystallogr.* **40**, s223-s228.

Sheldrick, G. (2010). *Acta Cryst*. D**66**, 479-485.

Svergun, D., Barberato, C., Koch, M. H. J. (1995). *J. Appl. Crystallogr.* **28**, 768-773.

Svergun, D. I. (1999). *Biophysical J.* **76**, 2879-2886.

Vagin, A. & Teplyakov, A. (2010). *Acta Cryst*. D**66**, 22-25.

Volkov, V. V., Svergun, D. I. (2003). *J. Appl. Crystallogr.* **36**, 860-864.

Winn, M. D. *et al.* (2011). *Acta Cryst*. D**67**, 235-242.